

# Determining Disturbance Recovery Conditions by Inverse Sensitivity Minimization

Michael W. Fisher, *Member, IEEE*

Ian A. Hiskens, *Life Fellow, IEEE*

**Abstract**—Power systems naturally experience disturbances, some of which can damage equipment and disrupt consumers. It is important to quickly assess the likely consequences of credible disturbances and take preventive action, if necessary. However, assessing the impact of potential disturbances is challenging because many of the influential factors, such as loading patterns, controller settings and load dynamics, are not precisely known. To address this issue, the paper introduces the concept of parameter-space recovery regions. For each disturbance, the corresponding recovery region is the region of parameter space for which the system will recover to the desired operating point. The boundary of the recovery region establishes the separation between parameter values that result in trouble-free recovery and those that incur undesirable non-recovery. The safety margin for a given set of parameter values is defined as the smallest distance (in parameter space) between the given values and the recovery boundary. Novel numerical algorithms with theoretical guarantees are presented for efficiently computing recovery boundaries and safety margins. Unlike prior methods, which tend to be overly conservative and restricted to low dimensional parameter space, these methods compute safety margins to arbitrary user-specified accuracy and do so efficiently in high dimensional parameter space. The efficacy of the methods is demonstrated using the IEEE 39-bus benchmark power system, where safety margins are computed for cases that consider up to 86 parameters, and reveal unexpected safety implications that would not have been observed otherwise.

## I. INTRODUCTION

Large disturbances, such as faults, are an inevitable part of power system operation, and in severe cases may lead to blackout conditions. In order to ensure safe and reliable operation, it is therefore important for power system operators to determine whether their system is vulnerable to credible disturbances. If the system is found to be vulnerable, i.e., the likelihood of recovery from potential disturbances is too small, system operators should take preventive action by manoeuvring the system to a safer operating point, thereby reducing the vulnerability.

Whether the system recovers from a particular disturbance to a desirable operating point depends upon many factors, including loading pattern, controller settings, and load characteristics. These factors usually appear in power system models as “known” parameters, though they are often not known

M. Fisher, michael.fisher@uwaterloo.ca, is with the Department of Electrical and Computer Engineering, University of Waterloo, 200 University Avenue West, Waterloo, ON N2L 3G1, Canada.

I. Hiskens, hiskens@umich.edu, is with the Department of Electrical Engineering and Computer Science, University of Michigan, 1301 Beal Avenue, Ann Arbor, MI 48109, U.S.A.

The authors gratefully acknowledge the contribution of the U.S. National Science Foundation through grant ECCS-1810144.

with absolute certainty. As a result, even if vulnerability to a potential disturbance has been assessed for a standard set of parameter values, those results may be unreliable and misleading due to the uncertainty inherent in the parameters of the actual system. Therefore, we first introduce a notion of safety margins for disturbance vulnerability assessment which quantitatively establishes the smallest change in parameter values, from their nominal values, that would result in the system failing to recover from the disturbance to the desired operating point.

The system is not vulnerable to a potential disturbance if clearance of that disturbance results in recovery to a desired operating point. The ability of the system to recover depends on the system parameter values. Therefore, we define the *recovery region* for a particular disturbance to be the set of parameter values for which the system will recover to the desired operating point. Furthermore, we define the *recovery boundary* to be the boundary of the recovery region in parameter space. For a given nominal set of parameter values, the *safety margin* is then defined as the distance from that nominal case to the recovery boundary. Thus, if perturbations from the nominal parameter set are less than the safety margin then the system is guaranteed to be able to recover from the disturbance. If parameter uncertainty is constrained to the recovery region then the system is guaranteed to recover from the specified disturbance.

In the special case where the parameter space under consideration is chosen to be the clearing time of a fault (and, thus, one dimensional), the recovery boundary will consist of the critical clearing time [1, Chapter 9], which is the maximum clearing time for which the system is just marginally unable to recover from a particular fault, and the safety margin will be the difference between the critical clearing time and the nominal clearing time. As the parameter space under consideration can be chosen to consist of any desired collection of system parameters, the definition of the recovery boundary can be thought of as a generalization of this notion of critical clearing time to arbitrary selections of parameters, thereby incorporating and quantifying the impact of parametric uncertainty on disturbance vulnerability.

Typical industry practice involves the construction of conservative approximations of the recovery boundary known as nomograms [2]. Such methods are typically limited to two- or three-dimensional parameter space. Several extensions to these traditional techniques have been proposed [3]. However, the number of computationally-intensive dynamic simulations required by these methods increases rapidly with parameter dimension. Consequently, they are still limited to low dimen-

sional parameter spaces and are constructed using off-line processes, with limited capability for updating to reflect real-time conditions. The small number of parameters of interest are chosen based on operational intuition and experience. Consequently, many parameters which could be critical to system recovery may be overlooked. This is particularly true given variability and uncertainty arising from renewable generation, controller settings, and load characteristics. Furthermore, existing methods are inherently approximate and can be overly conservative. Hence, it is desirable to develop techniques that offer more accurate and efficient computation of the recovery boundary, allowing rapid assessment of safety margins in higher dimensional parameter space.

Much of the classical work in rapid assessment of safety margins has focused on developing estimates of the region of attraction (RoA) of the desired operating point [1], [4]–[6]. However, as the exact identification of the RoA in high dimensional power system models is typically intractable, existing methods are inherently approximate and can be overly conservative. Some approaches attempt to reduce conservatism using knowledge of a particular equilibrium point, called the controlling unstable equilibrium point (CUEP), with specific dynamical properties. However, locating the CUEP can be challenging for high dimensional system models. In addition, the majority of existing methods for estimating safety margins focus on parameters which do not influence post-disturbance dynamics, such as the fault clearing time, which excludes many important system parameters. Finally, it is often unclear how to incorporate nonsmoothness, such as from saturation of controllers like the AVR and PSS, which can have a large influence on vulnerability.

Prior work [7], [8] developed efficient methods to numerically compute the recovery boundary to arbitrary precision in two-dimensional parameter space, and to determine safety margins in arbitrary dimensional parameter space. However, those methods require prior knowledge of the CUEP of a disturbance. Locating the CUEP for a particular disturbance is challenging, particularly when considering events such as controller saturation. Other prior work [9] required the numerical integration of additional high order dynamical systems, and was often inefficient or even intractable for high dimensional systems.

This paper develops novel, computationally efficient algorithms for numerically computing the recovery boundary in two-dimensional parameter space and determining safety margins in higher dimensional parameter space. These tools facilitate accurate, real-time assessment of disturbance vulnerability while capturing full nonlinear, non-smooth model details. The recovery boundary and safety margins are computed to arbitrary precision, so they are not conservative. Furthermore, they can incorporate any number and type of parameters. Crucially, these algorithms do not require prior knowledge of the CUEP, and therefore can be directly and efficiently applied to realistic power systems.

Computation of points on the recovery boundary relies on two key theoretical insights.

- 1) As parameter values from within the recovery region approach the recovery boundary in parameter space, the

post-disturbance initial condition in state-space, i.e., the system state at the instant the disturbance is cleared, approaches the region of attraction (RoA) boundary [1] of the desired equilibrium point. Therefore, to compute safety margins it suffices to find the closest parameter value to the given value whose corresponding post-disturbance initial condition lies on the RoA boundary in state space.

- 2) Since this post-disturbance initial condition lies on the RoA boundary, its trajectory is infinitely sensitive to small perturbations. This is because incremental changes in parameter values could push the trajectory either inside or outside the RoA, leading to very different asymptotic behavior.

Motivated by these ideas, the algorithms compute points on the recovery boundary by varying parameter values so as to maximize the trajectory sensitivities. This is accomplished by numerically computing the trajectory sensitivities, which are the derivatives of the trajectory with respect to parameter values. These sensitivities can be efficiently computed as a byproduct of numerically integrating the underlying system dynamics [10]. For implementation, however, it is numerically advantageous to minimize the inverse sensitivities rather than maximizing them directly. These ideas are applied to develop algorithms for numerically tracing the recovery boundary in two-dimensional parameter space, and for finding safety margins in higher dimensional parameter space.

The algorithms are demonstrated on the IEEE 39-bus benchmark power system. They are used to compute safety margins in three cases that have parameter space dimensions of 38, 76 and 86, respectively. This investigation reveals unexpected dynamic behavior, with important safety implications, which would not have been otherwise observed.

The paper is organized as follows. Section II provides the theoretical setting and justification for the algorithms, with the details of the algorithms then given in Section III. Section IV introduces the IEEE 39-bus benchmark power system test case, and Section V demonstrates the algorithm characteristics. Section VI offers concluding remarks.

## II. THEORY

### A. Model

Power systems exhibit dynamic behavior which consists of periods of smooth dynamics interspersed with discrete events, such as controllers encountering saturation limits. Such behavior is commonly modeled as a system of switched differential and algebraic equations (switched DAEs):

$$\dot{x} = f(x, y) \quad (1)$$

$$0 = g(x, y) \Leftrightarrow \begin{cases} g_i^+(x, y), & s_i(x, y) > 0 \\ g_i^-(x, y), & s_i(x, y) < 0, \end{cases} \quad (2)$$

where  $g$  is composed of sets of switched algebraic equations  $g_i^+, g_i^- : \mathbb{R}^{n+m} \rightarrow \mathbb{R}^{m_i}$ , with  $\sum_i m_i = m$ , and the composition is determined by the signs of the corresponding switching indicator functions  $s_i : \mathbb{R}^{n+m} \rightarrow \mathbb{R}$  whose zero level sets describe the switching surfaces, the dynamic states

$x \in \mathbb{R}^n$  represent quantities such as rotor angles and frequencies whereas the algebraic states  $y \in \mathbb{R}^m$  represents quantities such as bus voltages and line currents. Dynamics are driven by  $f : \mathbb{R}^{n+m} \rightarrow \mathbb{R}^n$ . It is quite realistic to assume that  $f$ ,  $g_i^+$ , and  $g_i^-$  are continuously differentiable. Note that switching occurs whenever  $s_i$  passes through zero, i.e., a switching surface is encountered, but otherwise, away from switching surfaces, the dynamics are smooth. Such hybrid dynamical systems accurately reflect realistic power system behavior.

The desired steady state operating point is given by a stable equilibrium point (SEP) of (1)-(2) which has an associated RoA. Consider a particular disturbance, and let the post-disturbance initial condition  $x_0$  be the system state at the instant when the disturbance clears. Let  $\mathbb{R}^P$  be a space of parameters of the system, and let  $p \in \mathbb{R}^P$  denote a vector of parameter values. As  $p$  varies, so do the RoA and the post-disturbance initial condition  $x_0(p)$ , with  $x_0 : \mathbb{R}^P \rightarrow \mathbb{R}^n$  capturing this parametric influence. Let  $x(p, x_0(p), t)$  denote the dynamic states in the solution of (1)-(2) at time  $t$  for parameter value  $p$  and initial condition  $x_0(p)$ .

### B. Trajectory sensitivities

Trajectory sensitivities are partial derivatives of the time varying states with respect to initial conditions and/or parameters. It is shown in [10], [11] that they can be efficiently computed as a byproduct of the numerical integration of the underlying dynamics for the switched DAEs of (1)-(2). For the vector of parameters  $p$ , define the trajectory sensitivities  $\chi$  of the dynamic states  $x$  with respect to  $p$  as:

$$\chi(p, t) := \frac{\partial x(p, x_0(p), t)}{\partial p}, \quad (3)$$

i.e., the partial derivative of the dynamic states<sup>1</sup> of the system at time  $t$ , starting from the post-disturbance initial condition  $x_0(p)$ . These trajectory sensitivities measure the sensitivity of the system dynamic states along a trajectory to small changes in parameter value.

**Example.** To develop intuition for the behavior of trajectory sensitivities for parameter values near the recovery boundary, consider the simple example of a single machine infinite bus with classical machine dynamics [1]. The disturbance considered in this system is a fault which is modeled by setting the electrical torque to zero until the fault is cleared. Fig. 1 shows the sensitivity of the frequency to generator mechanical power as that power value approaches the recovery boundary. Observe that trajectory sensitivities grow considerably larger as the recovery boundary is approached.  $\square$

More generally, the intuition behind this observation is that at the recovery boundary, small perturbations in parameter values could push the trajectory to either side of the RoA boundary, i.e., either recovery from the disturbance or failure to recover. Hence, the trajectory becomes infinitely sensitive to small changes in parameter values.

<sup>1</sup>The trajectory sensitivities  $\frac{\partial y}{\partial p}$  of the algebraic states  $y$  with respect to parameters  $p$  can be similarly defined. Those sensitivities, however, are not used by the algorithms that are presented subsequently.

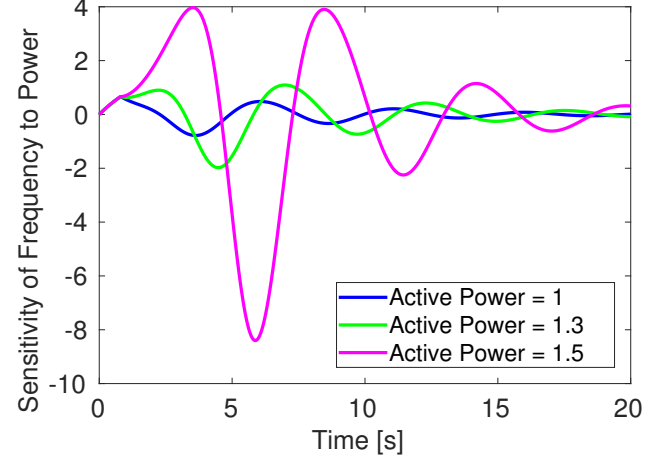


Fig. 1. Sensitivity of the post-fault frequency to generator mechanical power, as the generator power approaches the recovery boundary.

### C. Inverse sensitivities

To generalize the above intuition, define the scalar function  $G : \mathbb{R}^P \rightarrow \mathbb{R}$  by:

$$H(p, t) = \frac{1}{\|\chi(p, t)\|_1}, \quad (4)$$

$$G(p) = \inf_{t \geq 0} H(p, t), \quad (5)$$

where the matrix norm is defined by  $\|M\|_1 = \sum_{i,j} |M_{ij}|$  for any matrix  $M$ . Hence,  $G(p)$  represents the minimum over time of the inverse of the norm of the trajectory sensitivities. It follows that trajectory sensitivities diverging to infinity is equivalent to  $G$  approaching zero. Under practical assumptions, for a large class of nonlinear systems, the following result has been proven in [12, Theorem 1]:

**Theorem 1.** The function  $G$  is well-defined, continuous, and strictly positive over the recovery region, for  $p^*$  in the recovery boundary almost everywhere  $G(p^*) = 0$ , and for any convergent sequence of parameter values  $\{p_k\}_{k=1}^{\infty}$  in the recovery region, if  $\lim_{k \rightarrow \infty} G(p_k) = 0$  then  $\lim_{k \rightarrow \infty} p_k$  lies on the recovery boundary.  $\square$

In particular, Theorem 1 implies that solving for  $p$  such that  $G(p) = 0$  will drive  $p$  onto the recovery boundary. Furthermore, Theorem 1 also implies that, up to a set of measure zero, the recovery boundary is equal to  $G^{-1}(0)$ . These motivate the development of algorithms for computing points on the recovery boundary.

In order to develop algorithms for solving  $G(p) = 0$ , we require the derivative  $DG(p)$ . Note that,

$$DG(p) = \begin{bmatrix} \frac{\partial G}{\partial p_1}(p) & \frac{\partial G}{\partial p_2}(p) & \dots & \frac{\partial G}{\partial p_P}(p) \end{bmatrix}. \quad (6)$$

For any parameter  $p$  that lies inside the recovery region, by the proof of [12, Theorem 1] there exists a time  $\hat{t}(p)$  such that,

$$G(p) = \min_{t \geq 0} H(p, t) = H(p, \hat{t}(p)). \quad (7)$$

Since  $\hat{t}(p)$  is the point in time at which  $H(p, t)$  achieves a minimum, it is an extremal point of  $H(p, t)$  which implies,

$$\frac{\partial H}{\partial t}(p, \hat{t}(p)) = 0. \quad (8)$$

From (7),

$$\begin{aligned} \frac{\partial G}{\partial p_j}(p) &= \frac{\partial}{\partial p_j} \left( H(p, \hat{t}(p)) \right) \\ &= \frac{\partial H}{\partial p_j}(p, \hat{t}(p)) + \frac{\partial H}{\partial t}(p, \hat{t}(p)) \frac{\partial \hat{t}}{\partial p_j}(p) \\ &= \frac{\partial H}{\partial p_j}(p, \hat{t}(p)), \end{aligned} \quad (9)$$

where the last step follows by substituting in (8). So, to compute  $DG$  it suffices to compute  $\frac{\partial H}{\partial p_j}$ . To do so, define the following notation for  $i, j \in \{1, 2, \dots, P\}$ :

$$\begin{aligned} \chi_{[i]}(p, t) &:= \frac{\partial x}{\partial p_i}(p, x_0(p), t), \\ \chi_{[ij]}(p, t) &:= \frac{\partial^2 x}{\partial p_i \partial p_j}(p, x_0(p), t), \end{aligned}$$

where  $\chi_{[i]}(p, t)$  and  $\chi_{[ij]}(p, t)$  are both  $n$ -dimensional vectors<sup>2</sup>. Then  $\frac{\partial H}{\partial p_j}$  is given by,

$$\frac{\partial H}{\partial p_j}(p, t) = -\frac{\sum_{i=1}^P \text{sign}(\chi_{[i]}(p, t))^T \chi_{[ij]}(p, t)}{\|\chi(p, t)\|_1^2}, \quad (10)$$

where for any vector  $v$ ,  $(\text{sign}(v))_i = 1$  if  $v_i \geq 0$  and  $(\text{sign}(v))_i = -1$  if  $v_i < 0$ . As mentioned earlier, first-order trajectory sensitivities  $\chi_{[i]}$  can be computed efficiently as a byproduct of the underlying numerical integration. This is also the case for second-order sensitivities  $\chi_{[ij]}$ , as shown in [9], [11]. Combining (6), (9) and (10) therefore enables efficient computation of  $DG(p)$ .

### III. ALGORITHMS

Based on Theorem 1, the recovery boundary consists precisely of the parameter values  $p$  such that  $G(p) = 0$ . This section formulates algorithms for, 1) finding a point on the recovery boundary in the case of one-dimensional parameter space, 2) numerically tracing the recovery boundary in two-dimensional parameter space, and 3) finding the closest point on the recovery boundary in higher dimensional parameter space.

#### A. One-dimensional parameter space

To find a point on the recovery boundary, the goal is to solve,

$$G(p) = 0. \quad (11)$$

Earlier theoretical work [13] and numerical experiments [14] suggest that  $G$  is approximately affine for parameter values near the recovery boundary. Motivated by this linear structure, we solve (11) using Newton-Raphson with backtracking,

<sup>2</sup>Note that  $\chi_{[ij]}(p, t)$  differs from standard notation where  $\chi_{ij}(p, t) \equiv \frac{\partial x_i}{\partial p_j}(p, x_0(p), t)$ .

which is an iterative algorithm that converges rapidly for affine equations.

Let  $k$  be the latest iteration such that  $p^k$  lies in the recovery region. (At initialization,  $k = 0$  with  $p^0$  user specified.) The subsequent iteration  $i = k+1$  computes the updated parameter value  $p^i$  according to the Newton-Raphson step,

$$p^i = p^k - \mu G(p^k) / DG(p^k), \quad (12)$$

where  $\mu = (\frac{1}{2})^{i-k-1}$ . A full time-domain simulation is performed using parameter values  $p^i$  to determine whether the system recovers to the SEP or not, hence establishing whether  $p^i$  lies within or outside the recovery region. The values for  $G(p^i)$  and  $DG(p^i)$  are also computed. If  $p^i$  lies within the recovery region then  $k$  is updated by setting  $k = i$  and  $i$  is reinitialized to  $i = k + 1$ . Otherwise,  $k$  remains unchanged and  $i$  is incremented,  $i = i + 1$ . The process then repeats.

The algorithm ensures that  $\mu = 1$  for the first step beyond iteration  $k$ , so the full Newton-Raphson update is considered. However, if that results in progressing beyond the recovery region then the step length  $\mu$  is halved. This achieves a backtracking line search along the Newton-Raphson direction until a parameter value inside the recovery region is obtained.

Performing the update of (12) requires computation of  $G$  and its derivative  $DG$ , which proceeds as follows. During a time-domain simulation corresponding to parameter value  $p^k$ , the time  $\hat{t}(p^k)$  at which  $H(p^k, t)$  achieves its minimum (over time) is observed. Then  $G(p^k) = H(p^k, \hat{t}(p^k))$ , and  $DG(p^k)$  is computed using (6), (9) and (10) with  $P = 1$ . These are then used to perform the update of (12) to compute  $p^i$ .

This process is repeated iteratively until  $G(p^k)$  converges towards zero, which causes  $p^k$  to converge to the recovery boundary. This outcome is guaranteed by the following theorem, which was proven in [12, Theorem 2] under similar assumptions as in Section II:

**Theorem 2.** For  $p^0$  sufficiently close to the recovery boundary, the sequence  $\{p^k\}_{k=0}^{\infty}$  generated by (12) is well-defined and will converge to a unique parameter value on the recovery boundary.  $\square$

As with any numerical computation, satisfaction of (11) can only be achieved up to a small convergence tolerance  $\epsilon > 0$ . In other words, it is only possible to numerically compute  $p^*$  such that  $|G(p^*)| \leq \epsilon$ , rather than realizing  $G(p^*) = 0$  exactly. The same is true for the algorithms presented in Sections III-B and III-C, where  $\epsilon > 0$  will be the tolerance chosen such that the solution  $p^*$  satisfies  $|G(p^*)| \leq \epsilon$ .

#### B. Two-dimensional parameter space

By Theorem 1, the recovery boundary is equal to  $G^{-1}(0)$ . In two-dimensional parameter space,  $G : \mathbb{R}^2 \rightarrow \mathbb{R}$  is a scalar equation with two free variables (parameters). Because the number of free variables exceeds the number of equations by one, the recovery boundary is typically a one-dimensional curve. The goal is to numerically trace this curve  $G^{-1}(0)$  by iteratively computing a sequence of points that lie along the curve. This is accomplished using the following continuation method, which alternates between a predictor step and a

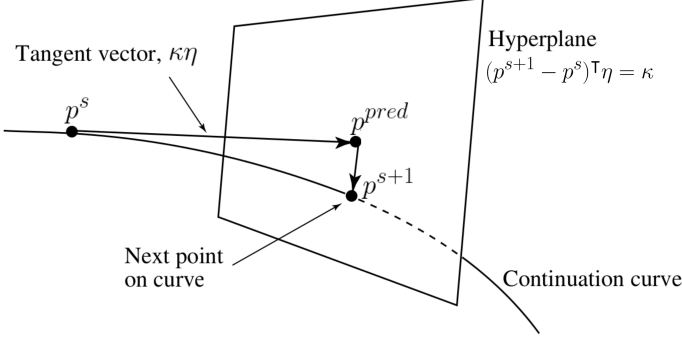


Fig. 2. The predictor-corrector continuation process for iteratively tracing a sequence of points along a curve.

corrector step, as shown in Fig. 2. Let  $s$  denote the current point on the curve, and  $p^s$  be the corresponding parameter values. Then  $p^s$  must satisfy  $G(p^s) = 0$ .

The predictor step generates a first order prediction of the next point on the curve, and proceeds as follows. First, we obtain the unit tangent vector to the curve  $G^{-1}(0)$  at  $p^s$ . This can be done by noting that  $DG(p^s)$  is orthogonal<sup>3</sup> to the curve  $G^{-1}(0)$ . Hence, any vector orthogonal to  $DG(p^s)$  must be tangent to  $G^{-1}(0)$  since the parameter space is exactly two-dimensional. We can compute  $DG(p^s)$  at each iteration using (6), (9) and (10) for  $P = 2$ . Then, writing  $DG(p^s) = [a \ b]$ , a tangent vector to the curve is given by  $[b \ -a]^\top$ . Let  $\eta$  denote  $[b \ -a]^\top$  divided by its norm, so that  $\eta$  is the unit vector tangent to the curve. Let  $\kappa \in \mathbb{R}$  be the step size for the prediction. Therefore the predicted point is given by,

$$p^{\text{pred}} = p^s + \kappa\eta. \quad (13)$$

Once a predicted point has been obtained, the next step is to correct back onto the curve  $G^{-1}(0)$ . To do so, an orthogonal projection from the predicted point onto the curve is performed. In particular, the next point on the curve  $p^{s+1}$  is chosen such that the vector  $(p^{s+1} - p^{\text{pred}})$  is orthogonal to the vector  $(p^{\text{pred}} - p^s)$ , so that,

$$(p^{s+1} - p^{\text{pred}})^\top (p^{\text{pred}} - p^s) = 0.$$

Using (13) and the fact that  $\eta$  is a unit vector, so  $\eta^\top \eta = 1$ , the above constraint simplifies to,

$$(p^{s+1} - p^s)^\top \eta - \kappa = 0. \quad (14)$$

Therefore, correction back onto the curve requires solution of the system of equations:

$$F(p^{s+1}) := \begin{bmatrix} G(p^{s+1}) \\ (p^{s+1} - p^s)^\top \eta - \kappa \end{bmatrix} = 0. \quad (15)$$

For notational convenience, replace  $p^{s+1}$  by  $\varphi$ . Solution of  $F(p^{s+1}) \equiv F(\varphi) = 0$ , which consists of two equations with two free variables (parameters), can again be achieved using Newton-Raphson with backtracking:

$$\varphi^i = \varphi^k - \mu DF(\varphi^k)^{-1} F(\varphi^k) \quad (16)$$

<sup>3</sup>Because  $G$  is constant along the curve, its derivative  $DG$  must be orthogonal to it.

where  $\mu = (\frac{1}{2})^{i-k-1}$ , iteration indices  $i, k$  are updated iteratively as in (12) and,

$$DF(\varphi) = \begin{bmatrix} DG(\varphi) \\ \eta^\top \end{bmatrix}.$$

At each iteration, if  $p^{\text{pred}}$  lies in the recovery region then set  $\varphi^1 = p^{\text{pred}}$ . Otherwise, if  $p^{\text{pred}}$  does not lie in the recovery region, then we perform a line search along the line (14) using, for example, the bisection or golden section search methods, to find a parameter value on (14) that lies in the recovery region, and set  $\varphi^1$  equal to that parameter value. Then, we proceed with the continuation process using the update (16) at each iteration. Upon convergence, Newton-Raphson will provide  $\varphi \equiv p^{s+1}$  such that  $F(p^{s+1}) = 0$ , which ensures that  $G(p^{s+1}) = 0$ , so  $p^{s+1}$  is on the curve  $G^{-1}(0)$ . This is guaranteed by the following theorem, which was proven in [12, Theorem 3] under similar assumptions as in Section II:

**Theorem 3.** For  $p^s$  satisfying  $G(p^s) = 0$  and  $\kappa > 0$  sufficiently small almost everywhere, and for  $\varphi^1$  contained in the hyperplane (14) and in the recovery region, the sequence  $\{\varphi^k\}_{k=1}^\infty$  generated by (16) is well-defined and will converge to a unique  $p^{s+1}$  that lies in the hyperplane (14) and on the recovery boundary.  $\square$

The prediction and correction steps then alternate until the recovery boundary has been traced.

### C. Higher dimensional parameter space

Now suppose that  $P > 2$ , so that  $G^{-1}(0)$  may be more than two-dimensional. (Recall that  $G^{-1}(0)$  typically has dimension equal to the number of free variables (parameters) minus the number of constraints, in this case one scalar equation.) Therefore, rather than tracing the recovery boundary, in this section our goal will be to find the closest point on the multi-dimensional recovery boundary to an initial parameter value. This will provide a quantitative measure of the margin for safe operation in the sense that it provides the smallest change in parameter values that would lead to a failure to recover from the disturbance.

Let  $p_0$  be any given initial parameter value, such as the current system conditions. Our objective is to find  $p \in G^{-1}(0)$  of minimum distance from  $p_0$ , where we consider Euclidean distance (2-norm)<sup>4</sup>  $\|p - p_0\|_2$ . This can be formulated as the optimization problem:

$$\begin{aligned} \min_{p \in \mathbb{R}^P} \quad & \frac{1}{2} (p - p_0)^\top (p - p_0) \\ \text{s.t.} \quad & G(p) = 0, \end{aligned} \quad (17)$$

where  $(p - p_0)^\top (p - p_0) = \|p - p_0\|_2^2$ . In general  $G$  is nonconvex, so (17) is a nonconvex optimization problem that is challenging to solve. However, historical work [13], [14], as well as our own numerical experiments (see Fig. 4), suggest that  $G$  is approximately affine near the recovery boundary. Therefore, we approximate  $G(p)$  locally by its linearization

<sup>4</sup>Note that Theorem 4, as proven in [12], holds for more general norms of the form  $(p - p_0)^\top A(p - p_0)$ , where  $A$  is symmetric positive definite.

and solve a sequence of quadratic programs [15]. In particular, at each iteration  $k$  we replace the nonlinear constraint  $G(p^{k+1}) = 0$  with the corresponding affine constraint obtained by linearizing  $G$  at  $p^k$ :

$$DG(p^k)(p^{k+1} - p^k) + G(p^k) = 0.$$

This gives the quadratic program,

$$\begin{aligned} \min_{p^{k+1} \in \mathbb{R}^P} \quad & \frac{1}{2}(p^{k+1} - p_0)^\top (p^{k+1} - p_0) \\ \text{s.t.} \quad & DG(p^k)(p^{k+1} - p^k) + G(p^k) = 0. \end{aligned} \quad (18)$$

The Lagrangian for this problem is given by,

$$\begin{aligned} \mathcal{L}(p^{k+1}, \lambda^{k+1}) = \frac{1}{2}(p^{k+1} - p_0)^\top (p^{k+1} - p_0) \\ + \lambda^{k+1}(DG(p^k)(p^{k+1} - p^k) + G(p^k)), \end{aligned}$$

where  $\lambda^{k+1}$  is a scalar Lagrange multiplier. The KKT conditions for an optimal solution yield,

$$0 = \nabla \mathcal{L}(p^{k+1}, \lambda^{k+1}) = \begin{bmatrix} p^{k+1} - p_0 + DG(p^k)^\top \lambda^{k+1} \\ DG(p^k)(p^{k+1} - p^k) + G(p^k) \end{bmatrix}.$$

Rearranging, the solution is given by the linear system,

$$\begin{bmatrix} I & DG(p^k)^\top \\ DG(p^k) & 0 \end{bmatrix} \begin{bmatrix} p^{k+1} \\ \lambda^{k+1} \end{bmatrix} = \begin{bmatrix} p_0 \\ DG(p^k)p^k - G(p^k) \end{bmatrix},$$

which can be efficiently solved numerically, with  $G(p^k)$  and  $DG(p^k)$  computed using (6), (9) and (10) following numerical integration of the first and second order trajectory sensitivities.

If  $p^{k+1}$  lies outside of the recovery region, which is determined as a byproduct of the simulation required to compute  $G(p^{k+1})$  and  $DG(p^{k+1})$ , then we instead move to the point  $p^k + \mu(p^{k+1} - p^k)$ , where  $\mu \in (0, 1)$  is determined by a backtracking line search that reduces by a factor of two at each iteration until the recovery region is encountered, as in Section III-A.

Sequential quadratic programming is repeated iteratively until the sequence of parameters converges to the optimal solution of (17). This outcome is guaranteed by the following theorem, which was proven in [12, Theorems 4-5] under similar assumptions as in Section II:

**Theorem 4.** For  $p_0$  sufficiently close to  $\partial R$  almost everywhere, there exists a unique solution  $p^*$  to (17). Furthermore, the sequence  $\{p^k\}_{k=1}^\infty$  starting from  $p^1 = p_0$  and generated by solving (18) and using a backtracking line search converges to  $p^*$ .

#### IV. EXAMPLE

The IEEE 39-bus benchmark test case [16], shown in Fig. 3, will be used to illustrate the algorithms of Section III. Generators are modeled using the 4th-order machine model from [1], while AVR and PSSs are modeled according to the IEEE standard [17] ST1C and PSS1A models, respectively. The full set of dynamic equations and system parameters are given in [16]. It is important to note that the nonsmooth AVR/PSS controller limits are included in this system model, which is vitally important for meaningful vulnerability assessment. The network is subject to a three-phase fault at bus 16, with fault

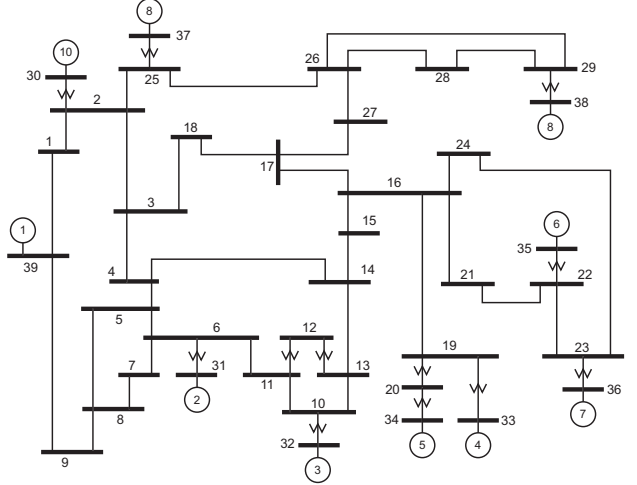


Fig. 3. IEEE 39-bus benchmark power system.

clearing at 0.2 s. The fault is modeled as a switched shunt reactance,  $X_{fault} = 0.001$  p.u.

Many model parameters of the system are of interest for recovery considerations. A load scaling factor is introduced which multiplies the active and reactive power loads at every bus in the network. As load is often uncertain, it is a natural choice for assessing system recoverability. An AVR gain scaling factor multiplies the AVR gain for every generator, and helps to capture the impact of controller tuning on system stability. The active and reactive power loads are represented by the standard exponential form of voltage dependent load model. The voltage exponents for all active-power loads are set equal, likewise for all reactive-power loads. As load dynamics are notoriously difficult to model, these parameters serve to capture the impact of uncertain load behavior on system recoverability.

#### V. RESULTS

The algorithms of Section III were demonstrated on the benchmark test case of Section IV. The dynamic states used in the formation of the function  $H$  in (4), and hence  $G$  in (5), were restricted to the generator dynamic states to avoid the possibility of the sensitivities of controller states dominating the sensitivities of the physical generator states.

The algorithm for one-dimensional parameter space, which finds a point on the recovery boundary, was applied with the parameter of interest being the load scaling factor. Fig. 4 shows that the algorithm converged to the recovery boundary in just 2 iterations (3 simulations total). Furthermore, it shows that  $G$  is approximately linear near the recovery boundary, both when the scaling factor is low (near 0.99) and high (near 1.06). The algorithm rapidly and accurately determines points on the recovery boundary in one-dimensional parameter space.

To observe the progression towards instability, note that generator 5 is the first generator to go unstable under stressed conditions. Fig. 5 shows the relative angle of generator 5 as a function of time for the values of the load scaling factor that were attained at each iteration of the algorithm, i.e., the points shown in Fig. 4. Observe that as the load scaling factor

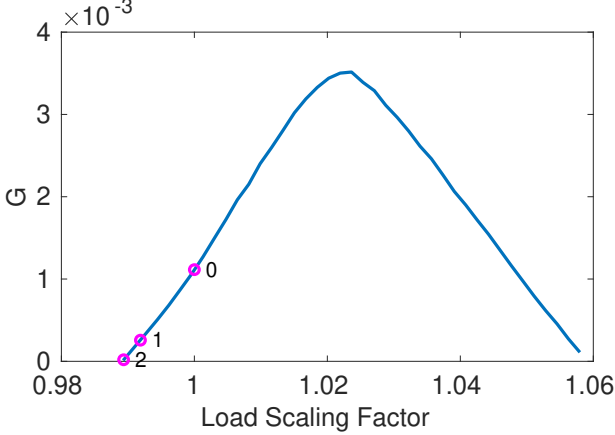


Fig. 4.  $G$  as a function of load scaling factor (blue line). The iterations of the one-dimensional parameter space algorithm are identified by circles and the iterations are labeled.

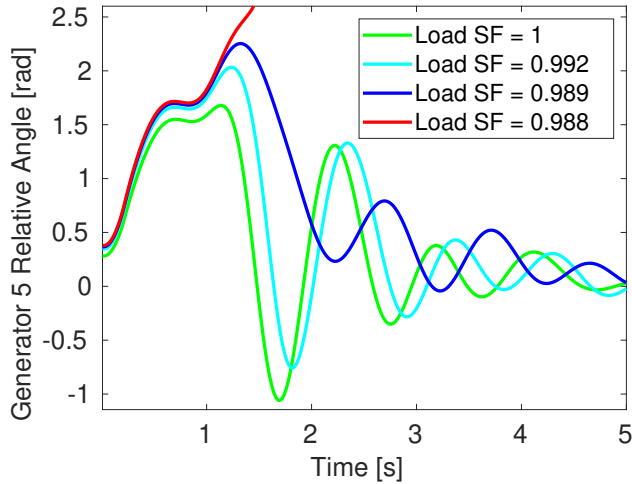


Fig. 5. The angle of generator 5 relative to generator 2 for the load scaling factor attained at each iteration of the one-dimensional algorithm. These values are shown in Fig. 4.

approaches the recovery boundary, the initial fluctuations in the relative angle of generator 5 grow larger, indicative of proximity to instability.

Once a point on the recovery boundary has been identified, the continuation method described in Section III can be applied to numerically trace the recovery boundary in two-dimensional parameter space. This algorithm was applied for the two-dimensional parameter space consisting of the AVR gain scaling factor and the reactive load voltage exponent. The tolerance was set to  $\epsilon = 10^{-5}$ . Fig. 6 shows the recovery boundary, and hence recovery region, in this parameter space. If the AVR gain scaling factor is reduced to around 0.8, i.e., gains are reduced by around 20%, the system will recover regardless of the reactive load exponent. However, for higher values of the AVR gain scaling factor, a nonempty region outside the recovery region emerges. For such cases, a wide range of reactive load voltage exponent values lie outside the recovery region. For example, if reactive loads exhibit constant

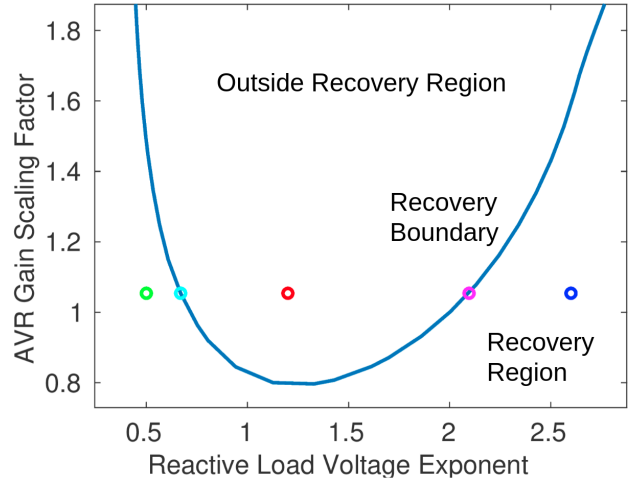


Fig. 6. The recovery boundary and recovery region in the two-dimensional parameter space of AVR gain scaling factor and reactive load voltage exponent. Colored circles indicate the parameter values whose corresponding dynamic behavior is shown in Fig. 7.

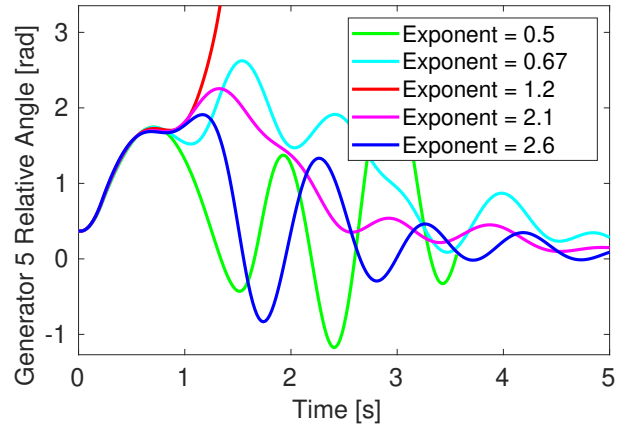


Fig. 7. The angle of generator 5 relative to generator 2, for an AVR gain scaling factor of 1.054 and the reactive load voltage exponents identified in Fig. 6.

current to constant voltage characteristics (voltage exponents in the range 1 to 2, respectively) and AVR gains are around their nominal values (scaling factor close to 1) then the system will not be able to recover from the fault. In contrast, as reactive loads approach constant power characteristics (voltage exponent around 0), the system becomes more resilient and is able to recover from the fault. These observations run counter to standard intuition, which suggests that constant power loads have a more detrimental impact on system stability. This counter-intuitive behavior serves as an example of the potential offered by these algorithms for revealing dynamic behavior which would not otherwise have been anticipated.

To observe the influence of reactive load voltage exponents on system recovery, recall that generator 5 is the first generator to go unstable as a result of the fault. Fig. 7 shows the relative angle of generator 5 as a function of time for a fixed AVR gain scaling factor of 1.054 and for several reactive load voltage

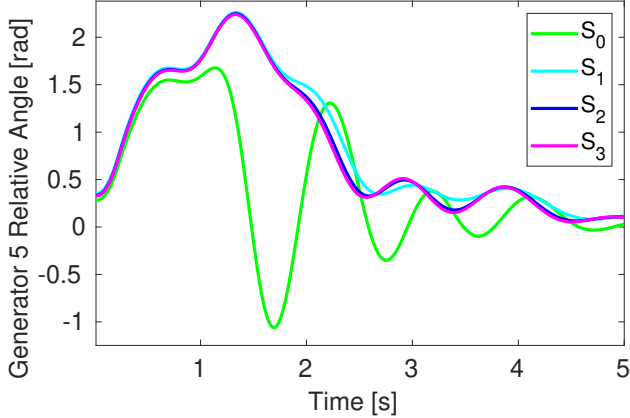


Fig. 8. The angle of generator 5 relative to generator 2 for the solutions of the optimization algorithm for parameter sets  $S_1$ ,  $S_2$  and  $S_3$ , as well as for the nominal parameter values  $S_0$ .

exponent values identified in Fig. 6. For sufficiently high or low exponents, the angle shows smaller initial fluctuations and a more rapid return to synchrony. For exponents near the recovery boundary, initial fluctuations are larger and take a longer time to damp before resynchronization. For exponent values between these recovery boundary values, the system loses synchronism and is unable to recover from the fault. Hence, for intermediate voltage exponents, angle fluctuations exhibit instability, whereas high or low load voltage exponents result in recovery from the disturbance.

The optimization algorithm described in Section III-C was applied to find the smallest changes in the active and reactive load values, active and reactive load voltage exponents, and AVR gains that would result in inability to recover from the disturbance. Three parameter sets were considered:

- $S_1$ : The set of active and reactive load values, capturing load uncertainty. (38 parameters)
- $S_2$ : The set  $S_1$  together with the set of active and reactive load voltage exponents. This set captures the uncertainty not only in the load levels but also their dynamic characteristics. (76 parameters)
- $S_3$ : The union of  $S_2$  and the set of AVR gains. This illustrates the influence of controller response on system recoverability. (86 parameters)

The optimization was applied to each of these sets of parameter values, with the solution tolerance set to  $\epsilon = 10^{-5}$ . The algorithm converged for all of the parameter sets. Fig. 8 shows the dynamic response of the generator 5 relative angle for each of the optimal parameter sets, as well as for the nominal parameter values (denoted by  $S_0$ ). Notice that the angle trajectories for the optimal solutions all display similar behavior, in particular a larger initial fluctuation than is the case for the nominal parameter values. Such behavior is indicative of proximity to instability.

The optimization algorithm determines the parameter values which minimize the (square of the) Euclidean distance from the nominal parameter values  $p_0$  to the recovery boundary, which is described by  $G(p) = 0$ . Hence, the optimal value of

TABLE I  
PARAMETER SPACE DIMENSION, SAFETY MARGIN AND ITERATION COUNT FOR THE OPTIMIZATION ALGORITHM OF SECTION III-C.

Parameter Set	Dimension	Safety Margin	Iterations
$S_1$	38	0.0107	14
$S_2$	76	0.0079	31
$S_3$	86	0.0071	39

the objective function measures the safe operating margin of the system. Table I shows this optimal value, i.e., the safety margin, for each set of parameters. Introducing additional parameters increases the degrees of freedom for the optimal solution, ensuring the optimal value cannot increase. Consequently, the optimal value (safety margin) decreased when the parameter set was expanded from  $S_1$  to  $S_2$ , and again from  $S_2$  to  $S_3$ .

For all the various combinations of parameters, the optimization algorithm converged rapidly (in less than 40 iterations) to a set of parameter values on the recovery boundary which appears to be closest to  $p_0$ . This is an impressive outcome, given the parameter space dimensions are 38, 76 and 86.

Overall, the algorithms were successfully applied to the IEEE 39-bus benchmark power system to find a point on the recovery boundary in one-dimensional parameter space, to numerically trace the recovery boundary in two-dimensional parameter space, and to find the closest point on the recovery boundary in higher dimensional parameter space.

## VI. CONCLUSION

The paper introduces the concept of a recovery boundary as the boundary in parameter space which separates parameter values that induce post-disturbance dynamic recovery from those that result in failure to recover. This then motivates the definition of a safety margin for a given set of parameter values as the shortest distance (in parameter space) from the given values to the recovery boundary.

Efficient numerical algorithms with convergence guarantees are presented for numerically tracing the recovery boundary in two-dimensional parameter space, and for finding the closest point on the recovery boundary in high dimensional parameter space. This closest point establishes the safety margin. Unlike prior developments, these algorithms are not conservative or approximate, can include parameters which influence post-disturbance dynamics, do not require prior knowledge of the controlling unstable equilibrium point, and can include nonsmooth limits such as controller saturation. They are not limited to low dimensional parameter space and are well suited for efficiently computing safety margins of realistic power systems.

The algorithms are supported by a theoretical framework which established an equivalence between a point on the recovery boundary in parameter space and the corresponding post-disturbance initial condition on the boundary of the region of attraction in state space. Furthermore, this framework showed that the latter could be found by varying parameter values so as to minimize the inverse trajectory sensitivities.

These insights underpin the algorithms presented in the paper, and provide convergence guarantees for those algorithms under mild assumptions.

The algorithms were demonstrated on the IEEE 39-bus benchmark power system, where they were used to numerically trace the recovery boundary in two-dimensional parameter space and to find safety margins in high dimensional parameter space. The results revealed an unexpected influence of load voltage dependence on system recovery, insights that would not have been identified otherwise. The algorithms accurately and efficiently computed the safety margins in each of 38, 76 and 86 dimensional parameter spaces.

## REFERENCES

- [1] P. W. Sauer and M. A. Pai, *Power System Dynamics and Stability*, 1997.
- [2] J. D. McCalley, S. Wang, R. T. Treinen, and A. D. Papalexopoulos, “Security boundary visualization for systems operation,” *IEEE Transactions on Power Systems*, vol. 12, no. 2, pp. 940–947, 1997.
- [3] Y. V. Makarov, P. Du, S. Lu, T. B. Nguyen, X. Guo, J. W. Burns, J. F. Gronquist, and M. A. Pai, “PMU-based wide-area security assessment: Concept, method, and implementation,” *IEEE Transactions on Smart Grid*, vol. 3, no. 3, pp. 1325–1332, 2012.
- [4] H.-D. Chiang and L. F. C. Alberto, *Stability Regions of Nonlinear Dynamical Systems: Theory, Estimation, and Applications*. Cambridge University Press, 2015.
- [5] H.-D. Chiang, *Direct Methods for Stability Analysis of Electric Power Systems*. John Wiley & Sons, Inc., 2011.
- [6] R. T. Treinen, V. Vittal, and W. Kliemann, “An improved technique to determine the controlling unstable equilibrium point in a power system,” *IEEE Transactions on Circuits and Systems - I: Fundamental Theory and Applications*, vol. 43, no. 4, pp. 313–323, 1996.
- [7] M. W. Fisher and I. A. Hiskens, “Numerical computation of parameter-space stability/instability partitions for induction motor stalling,” *International Federation of Automatic Control - PapersOnLine*, vol. 49, no. 27, pp. 250–255, 2016.
- [8] ———, “Numerical computation of critical parameter values for fault recovery in power systems,” *2018 Power Systems Computation Conference (PSCC)*, pp. 1–6, 2018.
- [9] ———, “Numerical computation of critical system recovery parameter values by trajectory sensitivity maximization,” *58th Conference on Decision and Control (CDC)*, pp. 8000–8006, 2019.
- [10] I. A. Hiskens and M. A. Pai, “Trajectory sensitivity analysis of hybrid systems,” *Circuits and Systems, IEEE Trans. on*, vol. 47, no. 2, pp. 204–220, 2000.
- [11] S. Geng and I. A. Hiskens, “Second-order trajectory sensitivity analysis of hybrid systems,” *IEEE Transactions on Circuits and Systems I*, vol. 66, no. 5, pp. 1922–1934, 2019.
- [12] M. W. Fisher, “Computing safety margins of parameterized nonlinear systems for vulnerability assessment via trajectory sensitivities,” 2025, under review. Preprint available on arXiv.
- [13] S. Roy and I. A. Hiskens, “Inverse-affine dependence of recovery-time sensitivities on critical disturbance parameters: A nonlinear dynamics explanation,” *American Control Conference (ACC)*, pp. 4452–4456, 2012.
- [14] T. B. Nguyen, M. A. Pai, and I. A. Hiskens, “Computation of critical values of parameters in power systems using trajectory sensitivities,” *14th Power Systems Computation Conference (PSCC)*, pp. 1–6, 2002.
- [15] J. Nocedal and S. Wright, *Numerical Optimization*, 2nd ed. Springer, 2006.
- [16] R. Ramos, I.A. Hiskens, et al., “Benchmark systems for small-signal stability analysis and control,” IEEE Power and Energy Society, Tech. Rep. PES-TR18, 2015.
- [17] IEEE Std. 421.5-2016, *IEEE Recommended Practice for Excitation System Models for Power System Stability Studies*. New York: Institute of Electrical and Electronics Engineers, Inc., 2016.



**Michael W. Fisher** is an Assistant Professor in the Department of Electrical and Computer Engineering at the University of Waterloo, Canada. He was a postdoctoral researcher with the Automatic Control and Power System Laboratories at ETH Zurich. He received his Ph.D. in Electrical Engineering: Systems at the University of Michigan, Ann Arbor in 2020, and a M.Sc. in Mathematics from the same institution in 2017. He received his B.A. in Mathematics and Physics from Swarthmore College in 2014. His research interests are in dynamics, control, and optimization of complex systems, with an emphasis on electric power systems. He was a finalist for the 2017 Conference on Decision and Control (CDC) Best Student Paper Award and a recipient of the 2019 CDC Outstanding Student Paper Award.



**Ian A. Hiskens** is the Vennema Professor Emeritus in the Department of Electrical Engineering and Computer Science, University of Michigan, Ann Arbor, MI, USA. He has held prior appointments with the Queensland Electricity Supply Industry, and various universities in Australia and the United States. His research interests lie at the intersection of power system analysis and systems theory, with recent activity focused largely on integration of renewable generation and controllable loads. Dr. Hiskens is involved in numerous IEEE activities in the Power and Energy Society, Control Systems Society, Circuits and Systems Society, and Smart Grid Initiative, and was the VP-Finance of the IEEE Systems Council. He is the Editor-in-Chief of the *IEEE Transactions on Power Systems* and is a member of the Editorial Board of the *Proceedings of the IEEE*. Dr. Hiskens is a Life Fellow of IEEE, a Fellow of Engineers Australia, a Chartered Professional Engineer in Australia, and was the 2020 recipient of the M.A. Sargent Medal from Engineers Australia.